IAES International Journal of Artificial Intelligence (IJ-AI)
Vol. 15, No. 6, December 2026, pp. 5096~5112
ISSN: 2252-8938, DOI: 10.11591/ijai.v15.i6.pp5096-5112

EfficientNet–generative adversarial network with improved artificial hummingbird optimization for image deblurring

Rohini Ashok Bhadane[1], Amol D. Potgantwar[2]
[1]Department of Computer Science and Engineering, BKC's MET Institute of Engineering, affiliated to Savitribai Phule Pune University, Nashik, India
[2]Department of Computer Engineering, Sandip Institute of Technology and Research Center, affiliated to Savitribai Phule Pune University, Nashik, India

Article Info

Article history:

Received Sep 30, 2025
Revised Jul 18, 2026
Accepted Sep 19, 2026

Keywords:

Blur dataset
EfficientNet
Generative adversarial network
Image deblurring
Improved artificial hummingbird optimization

ABSTRACT

This study addresses the persistent challenge of image degradation caused by defocus, motion, and acquisition errors, which severely affect recognition and classification tasks. Existing deblurring techniques often face limitations in handling both spatially variant and invariant blurs, with deep learning-based models struggling with accuracy and computational overhead. To overcome these challenges, this study proposes an improved artificial hummingbird-based efficient generative adversarial network (IAh-EffGAN), which integrates EfficientNet into the generative adversarial network (GAN) architecture and optimizes the loss function through an improved artificial hummingbird (IAh) meta-heuristic algorithm. A cross-guided bilateral filter is first applied for artifact suppression, followed by the IAh-EffGAN model for precise deblurring. Experimental results on the Blur dataset determine that proposed framework achieves higher results, with peak signal-to-noise ratio (PSNR) of 48.344 dB and structural similarity index measure (SSIM) 99.05, outperforming state-of-the-art models such as scale-recurrent network (SRN), deep residual Fourier transformation (DeepRFT) and conventional GANs. Comparative analysis using perception-based image quality evaluator (PIQE), absolute mean sharpness error (AMSE) and entropy-based measures further validate the robustness of the proposed work. These results establish IAh-EffGAN as promising solution for enhancing image clarity in photography, medical imaging, and surveillance applications.

This is an open access article under the CC BY-SA license.

Corresponding Author:

Rohini Ashok Bhadane
Department of Computer Science and Engineering, BKC's MET Institute of Engineering
Affiliated to Savitribai Phule Pune University
Nashik-422003, Maharashtra, India
Email: rohinibhadane102@gmail.com

1. INTRODUCTION

The image deblurring is the task of restoring an image from blur by suppressing, or dismissing the disturbing effect on the imaging that lead to image blur. Identifying the origin of blur is still an open question in image restoration problems. Photograph, in the Cambridge Dictionary, is the art or practice of taking and printing photographs with a camera. In medical and healthcare research, visual fidelity is crucial for providing surgeons and doctors with confidence in the decision-making process [1]. Blurriness is common in images due to bokeh effect which results when the background of an image is out-of-focus because the subject being photographed is too close to the camera and a non-zero depth of field exists [2], [3]. In such cases, the unfocused background is a main source of blurring. Although bokeh is occasionally employed

deliberately to convey an artistic emphasis, it generally results in poorer image clarity and degraded visual interpretability. Pictures may also be unsharp due to errors on distance between the camera and the subject or a miscalculation of the sharpness plane.

Several techniques have therefore been devised to tackle image degradation caused by more than one source. The primary contributors of blur are motion, defocus, low illumination (except among the recently developed methods), noise, and lens variations or acquisition radiance variation [4]. Wang *et al.* [5] exploit the task priors to solve severe blur removal.

The automatic deblurring of severely blurred images is still a challenging problem despite labor-intensive studies. Large blurring can bring irreversible damage to information, and has driven the development of many deblurring algorithms at various computation levels. Most existing methods are usually based on machine learning models under the framework of computer vision to enhance restoration [6]. However, conventional digital image processing methods, such as filtering and wavelet transform and motion detection have also adopted for the restoration of blurred images with success [7]. Apart from photography, image restoration is an important issue in digital image processing since image degradation arises in various application fields such as photography, medical imaging [8], entertainment, and remote sensing.

Image deblurring is also a digital image and video post-processing operation. Visual data often appears out of focus due to camera motion, aperture settings, or improper subject distance. Deconvolution approaches have been specifically developed for the purpose of recovering spatial resolution lost due to imaging systems, and are well studied [9]–[11]. Blind image restoration methods also require unknown blur kernel that estimates directly the ambition from degraded images [12] and fall short to restore for three blockers, while motion deblurring techniques aim at rectifying distortions introduced by scene or camera movement during acquisition [13]. These methods have been successfully used to improve visual quality and interpretability in a variety of application domains [14].

Recently deep learning-based deblurring has proven to be a transformative research direction. convolutional neural networks (CNN) and various network architectures provide superior performance for blur, degradation, and noise reduction by learning adaptive filters from data [15], [16]. Results of deep learning provide significantly better preservation of fine structural details and improved perceived image quality than do conventional methods. Subsequent iterative refinement using back-propagation results in substantially improved restoration of sharp images from degraded input [17]. Additional improvements in image quality are achieved with normalization and contrast adjustment techniques. As a result, deep learning represents a highly effective tool for the solution of problems associated with image degradation in a variety of applications [18]. The need for restoration of image blur is not merely an aesthetic concern, but represents one of the major limitations for subsequent techniques of feature extraction, object recognition and scene interpretation [19]. Consequently, removal of image blur is of major importance as a pre-processing step for enhancement of the reliability and utility of visual information [19]. Finally, restoration of image blur is of major importance for operation of systems that rely on facial recognition [20]. In these applications, degradation of image quality attributable to differences in timing of operation of the various camera sensors is sufficient to impair performance of systems of security importance [20]. As a consequence, restoration of image blur represents an example of a fundamental and basic technological requirement.

Typically, sharp-edge predictor-based methods for image deblurring are heuristic and employ iterative coarse-to-fine strategies combined with gradient thresholding. However, these approaches suffer from limitations including sensitivity to internal parameters and high computational requirements for estimation of the blur kernel, thereby precluding application to resource-limited devices or for use in time-critical applications. To address these limitations, this study developed efficient deep learning-based methods. This study combined approach for suppression of artifacts and application of the optimal deep learning-based method eliminated all limitations of conventional methods. First, artifacts present in the degraded input were removed and subsequently synthesized by a generative adversarial network (GAN). The subsequent development of hybrid methods represented an additional important advance, achieved by incorporation of adaptive optimization strategies for image reconstruction.

In particular, maintenance of high quality and unaltered visual information is of critical importance for accurate clinical interpretation and diagnosis. The objectives of this study are as follows:

i) To remove blur from images using an improved artificial hummingbird-based efficient generative adversarial network (IAh-EffGAN).
ii) To filter artifacts using a cross-guided bilateral filter, which combines guided and bilateral filtering processes for improved image preprocessing.
iii) To enhance deblurring accuracy by incorporating EfficientNet within the generator module of the GAN, enabling superior feature extraction and reconstruction.
iv) To evaluate performance comprehensively by analyzing multiple metrics and comparing the proposed framework with state-of-the-art methods.

The subsequent sections of the paper are structured as follows: section 2 presents an overview of pertinent methodologies for image deblurring. Section 3 offers a concise overview and illustrations of the complete methodology employed for the image deblurring of the proposed model. Section 4 analyzes the overall performance of the proposed model in comparison to existing methodologies, illustrated using graphs. The comprehensive conclusion of the suggested model is detailed in section 5.

2. LITERATURE REVIEW

Blurred image restoration remains an active area of research, with classical and deep learning-based methods developed to restore images with greater perceptual clarity and fewer artifacts. Despite major successes, most existing methods continue to suffer from poor computational efficiency, limited noise robustness and poor generalization across different blur conditions. Here, this study describes some related work and limitations. Guo *et al.* [21] presented a scale-invariant variant-depth network (VDN) for motion deblurring, which consists of four sub-networks that can adjustably change its depth. The encoder deciphers features from the deuxp blurred images, and the decoder encapsulates them. However, due to the use of large convolutional layers in this approach, its computational complexity is high which made it difficult to apply the method for real-time scenarios despite being obtained competitive results on GoPro and HIDE datasets.

Zhu *et al.* [22] proposed the adaptive multi-scale fusion blind deblurred generative adversarial network (AMD-GAN) to solve different degrees of image blur by multi-scale feature fusion. Empirical results on datasets RealBlur-R show that the proposed method achieves better deblurring performance. But had a time complexity, which was high for the requirements where processing should be done in real-time. Karanwal and Diwakar [23] improved face recognition in the presence of noise and blur by introducing the noise and blur invariant local descriptor (NABILD). The structural details were well preserved by using the Gaussian white noise (GWN) and salt-and-pepper noise (SPN) along with the multiscale local phase quantization neighborhood intensity. However, its performances drop when illumination and occlusion conditions are varied, which still presents issues in real world face recognition. Souibgui *et al.* [24] proposed text-degradation-invariant autoencoder (TDIAE), a degradation-invariant autoencoder (DIAE) for text recognition and document image enhancement. This method utilized an encoder–decoder architecture to recover damaged or blurry text documents and obtained promising results on datasets like IAM, CVL, IIT5K, IC13. Although it was workable, its performance was unsatisfactory and time-consuming, especially in the case of large-scale document enhancement problems. The study by Flusser *et al.* [25] dealt with the problem of rotational motion blur invariants, for which he introduced geometric moment invariants for the rotating image. While their recognition invariance under rotational motion blur considerably improved, their effectiveness was restricted by brightness sensitivity and long exposure, which hampered efficiency in a dynamic environment. One can conclude from this review that, although image deblurring has significantly progressed with deep learning and descriptor-based methods, they were mostly computationally heavy [21], [22] or non-robust under varied conditions [23]–[25]. Also, the available GAN-based methods either produce artifacts or fail to generalize over both spatially varying and invariant blur cases. These deficiencies call for a more computationally efficient, optimization-driven framework that achieves complexity reduction, enhances accuracy, and maintains target details. Chai *et al.* [26] applied GAN-based techniques to improve image quality for construction-type images. In medical imaging applications, Reyes and Sánchez [27] investigated CNNs for brain tumor classification using magnetic resonance images, highlighting the relevance of deep visual feature learning in diagnostic image analysis and more recently, Jiang and Li [28] used a texture-aware loss function that provided substantially improved perceptual quality for applications of image super-resolution. These results confirm the great potential for future development of hybrid deep learning systems incorporating sophisticated optimization strategies and thus represent a strong stimulus for our development of the IAh-EffGAN method for highly robust and interpretable image deblurring.

This motivates the development of the proposed IAh-EffGAN model, which integrates EfficientNet for robust feature extraction, incorporates a cross-guided bilateral filter for artifact suppression, and leverages the improved artificial hummingbird (IAh) optimization algorithm to minimize information loss. The comparison results in Table 1 show that although existing work are novel, they suffer from high computational complexity [21], time inefficiency [22], [24] and sensitivity to the disturbance of environmental conditions such as light variation and occlusions [23], [25]. Further, they are not often well applicable to generalization over spatially variant and invariant blur. To address these limitations, here this study presents the IAh-EffGAN framework that employs EfficientNet for strong feature representation, applies a cross-guided bilateral filter to eliminate artifacts, and incorporates the IAh optimization algorithm to minimize loss of information. This hybrid vector leads to better deblurring accuracy and perceptual quality, and achieves state-of-the-art performance in terms of multiple evaluation measures compared with the existing methods.

Table 1. Survey about existing methods

Author and reference	Technique used	Dataset	Aim/contribution	Strengths	Limitations	Performance metrics
Guo *et al.* [21]	VDN	GoPro, HIDE	To reduce motion blur using variant-depth sub-networks	Flexible depth control, encoder–decoder design extracts detailed features	High computational complexity due to large convolutional layers	Peak signal-to-noise ratio (PSNR), structural similarity index measure (SSIM)
Zhu *et al.* [22]	Adaptive multi-scale fusion GAN (AMD-GAN)	RealBlur-R, Remote Sensing, Drone datasets	Enhance deblurring through multi-scale fusion of blurred image features	Effective multi-scale fusion, handles diverse blur levels	High time complexity, not suitable for real-time tasks	PSNR, SSIM, MAP, Precision, Recall
Karanwal and Diwakar [23]	NABILD	ORL Face Dataset	Face recognition under blur and noise variations	Robust against GWN and SPN	Sensitive to lighting variations and occlusions	Accuracy
Souibgui *et al.* [24]	Text-DIAE	IAM, CVL, IIT5K, IC13	Text recognition and document enhancement	Learns degradation-invariant representations, effective for damaged text images	High time complexity, reduced scalability	Accuracy, PSNR, DRD, FM
Flusser *et al.* [25]	Rotational motion blur invariants (geometric moments)	RSML-C	Recognition under rotational blur	Captures motion-based invariant features for rotation	Sensitive to brightness variations, requires longer exposure times	PSNR, SSIM, MAP, Precision, Recall
Proposed (IAh-EffGAN)	IAh-EffGAN	Blur Dataset (Kaggle)	Remove blur and artifacts, improve accuracy and generalization	Integrates EfficientNet for feature extraction, IAh optimizer reduces information loss, cross-guided bilateral filter removes artifacts	Slightly higher training complexity compared to classical models	PSNR: 48.34 dB, SSIM: 99.05, absolute mean sharpness error (AMSE): 1.55, perception-based image quality evaluator (PIQE): 98.57, Entropy: Spatial 4.38, Spectral 7.41

3. METHOD

Images of real-world scenes or objects may be degraded by various factors including errors in the acquisition process and optical conditions of inappropriate depth of field, incorrect focusing, camera instability and subject motion. This generally leads to production of low-contrast, noisy images with artifacts that impair performance on tasks of recognition or classification. In order to cope with it, deep learning has been actively using in image restoration, style transfer and super-resolution. This paper proposes new method called IAh-EffGAN as shown in Figure 1.

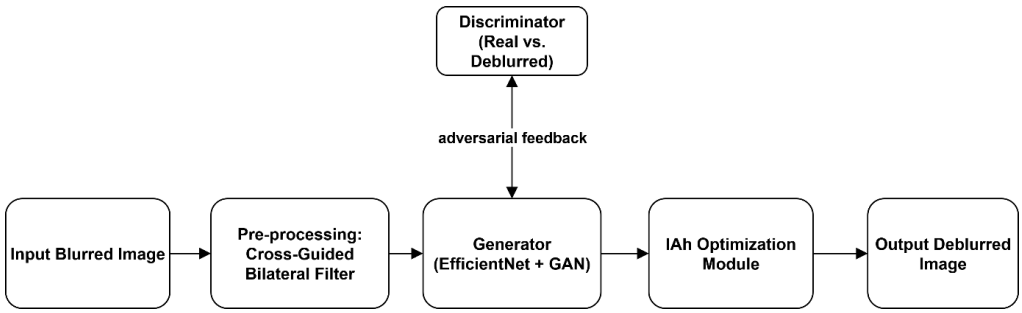

Figure 1. Architecture of proposed methodology

According to Figure 1, the process begins by sourcing the input image from the Blur dataset. The image undergoes filtration using the cross-guided bilateral filter to eliminate artifacts in the pre-processing

stage. Subsequently, the proposed IAh-EffGAN is employed to deblur the image. EffGAN is specifically designed by integrating EfficientNet into the GAN framework to improve deblurring performance. Additionally, the loss function optimization using the IAh algorithm aids in minimizing information loss and enhancing the generalization capacity of the classifier.

3.1. Preprocessing using the cross-guided bilateral filter

The pre-processing stage utilizes a cross-guided bilateral filter [29] to remove artifacts from the images. This filter is an iterative and robust method that combines properties of bilateral filtering with a weighted guided image. It calculates weights from detailed images derived from two different image types: guided and input images. Shaping the kernels with one of these images stabilizes edges while smoothing the filtered image, effectively eliminating lighting variations and weak noise details.

Figure 2 illustrates the cross-guided bilateral filter, which combines spatial and range kernels to filter out speckling noise, effectively removing image lighting variations. The filtered image is obtained as the result of this sequence, as shown in (1).

$$G_{cross-guidedbilateralfilter}(p,q) = H_{cross-guidedbilateralfilter} = \frac{1}{\omega}\sum_{P,Qe\in\omega P,Q} ks_{\sigma u}\,(|P-Q|)m_{\sigma V}(|H(P)-H(Q)|)H(Q) + c_{P,Q}X_{P,Q} + z_{P,Q} \quad (1)$$

Here, $|P-Q|$ is denoted as the distance between P and Q pixels, where P and Q are the two adjacent pixels, $H(P)$ and $H(Q)$ are the pixel positions, and $k$is denoted as the guided image weight. The spatial function and range Gaussian function are expressed in (2) and (3), respectively.

$$T_{\sigma t}|P-Q| = f^{\frac{(|H(P)-H(Q)|^2)}{2\sigma t^2}} \quad (2)$$

$$T_{\sigma D}(|H(P)-H(Q)|) = f^{\frac{(|H(P)-H(Q)|)^2}{2\sigma D^2}} \quad (3)$$

Here, σt and σD is denoted as the constraints, it controls the bilateral filtering process. $T_{\sigma t}$ is denoted as the spatial function, $T_{\sigma D}$ is denoted as the range Gaussian function. Cumulating σt means the smoothing of features that reduces the mean square error (MSE). The coefficient $c_{P,Q}$ and $z_{P,Q}$ as shown in (4) and (5).

$$c_{P,Q} = \frac{\frac{1}{\omega}\sum_{e\in\omega P,Q} X_M^e E_N^e - X_M^{P,Q} E_N^e}{\sigma P,Q^2+\varepsilon} \quad (4)$$

$$z_{P,Q} = E_N^e - c_{P,Q}X_M^{P,Q} \quad (5)$$

Here, $c_{P,Q}$ and $z_{P,Q}$ denotes the coefficients of guided filter, and mean of original, and guided images are E_N^e, and $X_M^{P,Q}$ also ω is the window function. The variance of the window σ_{P,Q^2} and ε is the regularization constant. Here cost function is represented in (6).

$$L(c_{P,Q}, z_{P,Q}) = \sum_{e\in\omega r}\left(c_{P,Q}X_M^e + z_{P,Q}E_N^e\right)^2 + \varepsilon c_{P,Q^2} \quad (6)$$

Finally, this filter eliminates an image lighting, and finds out the weak noise details in image and improve their quality.

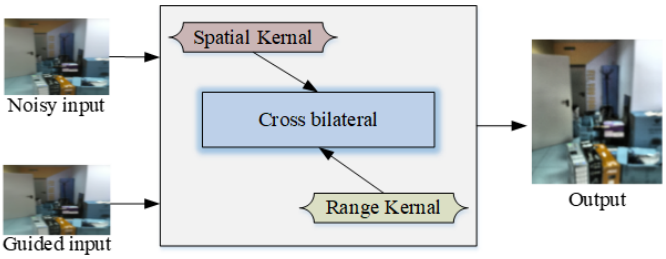

Figure 2. Cross-guided bilateral filter

3.2. Deblurring using the IAh-EffGAN model

Image deblurring using a GAN [26] with EfficientNet integrated into the generator represents a novel solution to restoring clear and sharp images from degraded inputs. The GAN is trained on pairs of blurry and sharp images and comprises two major components: the generator and the discriminator. The goal is to convert a blurry input image B into a sharp output image A. To achieve this, the EffGAN model is used, as shown in Figure 3.

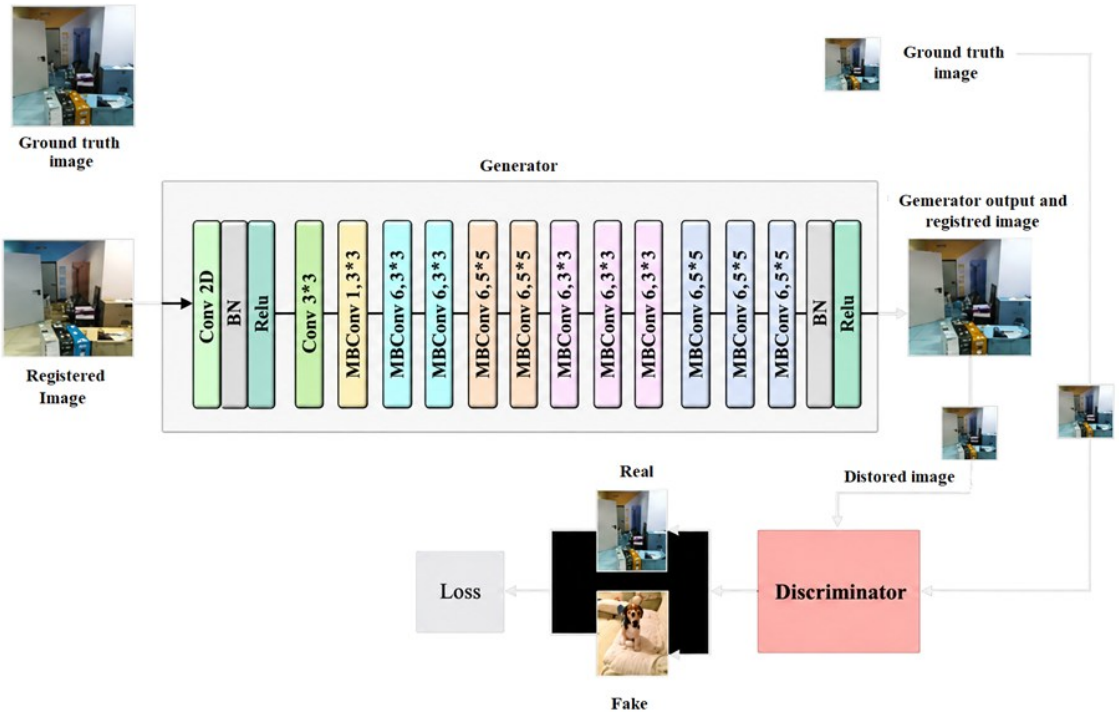

Figure 3. EffGAN model

Typically, the deblurred image X_{CD} generated by the GAN should match the sharp image according to (7). However, during the deblurring process applied to the pre-processed output, certain high-resolution details are lost, leading to artifacts in the deblurred output. Therefore, it's important to address this lost information in the conventional model.

$$B = (X_{CD} + \Delta X) \otimes G \tag{7}$$

Where ΔX is represented as the lost information of the deblurred image referred to as the IAh optimization technique. It aids in retrieving this lost information and mitigating information loss. Initially, the EffGAN is trained to estimate the X_{CD} corresponding to each blurred image B. Then IAh is performed to recover lost information ΔX, such as latent images $X = X_{CD} + \Delta X$. The schematic of the proposed deblurring model is shown in Figure 3.

3.2.1. Generator

The generator in EffGAN captures both low- and high-level features, enabling detailed information extraction from input images. It employs convolution 2-dimension (Conv2D) and mobile inverted bottleneck convolution (MBConv) block layers and integrates the B0 variant of EfficientNet, known for effective image feature representation. This enhances the generator's capacity to produce sharper and clearer outputs.

3.2.2. Discriminator

The discriminator shown in Figure 4 distinguishes between real and generated sharp images. It progressively reduces image resolution using Conv2D blocks, replaces dense layers with global average pooling to prevent overfitting, and applies a sigmoid function to classify outputs as real or fake. Its adversarial feedback drives the generator to iteratively improve.

Here, the proposed discriminator architecture closely resembles the structure of other GAN discriminators, such as that of the super-resolution generative adversarial network (SRGAN) model. Specifically, the initial Conv2D block of the discriminator consists of three kernels, 64 channels, and a stride of 1. As the processing progresses, kernel sizes increase from 64 to 256, with strides of 1 or 2, effectively reducing the resolution of the images. To prevent overfitting during training, the traditional dense layer is replaced with global averaging pooling. Finally, the decision on whether an image is genuine or generated is made using the sigmoid function. Overall, the EffGAN discriminator plays a crucial role in guiding the training of the generator toward producing clear and realistic images from blurry inputs. However, the EffGAN model obtained the cross-entropy loss in given as following section.

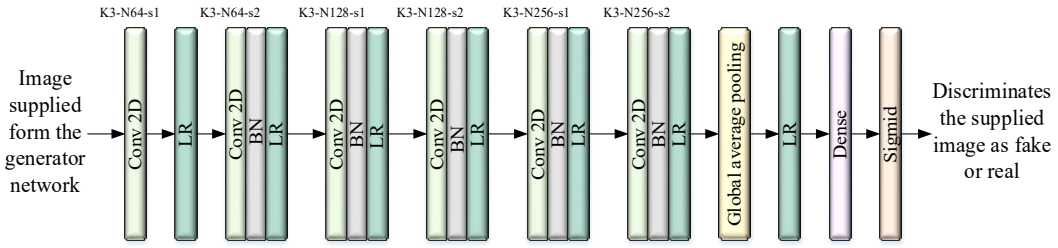

Figure 4. EffGAN discriminator

3.2.3. Loss function

The cross-entropy loss function used during adversarial training is expressed in (8).

$$M = \frac{1}{S}\sum_x M_x = \frac{1}{S}\sum_x \sum_{e=1}^{D} r_{xe}\, log(f_{xe}) \tag{8}$$

Here, D is denoted as the number of classes, r_{xe} is denoted as the discriminant function (0 or 1), which takes 1 when the true label class of the sample x is e and 0 otherwise, and f_{xe} is denoted as the probability that the sample x is predicted to be in class e. The proposed deblurring model integrates an IAh optimization algorithm to mitigate losses in the EffGAN model.

3.2.4. Improved artificial hummingbird optimization algorithm

While EffGAN provides strong results, some high-resolution details may still be lost. To overcome this, the IAh algorithm [30] is employed. Inspired by hummingbird foraging behaviors, it incorporates guided, territorial, and migration foraging strategies.

i) Initialization

A group of k hummingbirds are situated on k food sources (9), with their initial positions being random as detailed.

$$p_n = l + r(u - l) n = 1, \ldots . k \tag{9}$$

Here, p_n represents the location of the k food sources, l and u marks the lower boundary and upper boundary, and r specifies the vector within the interval of [0, 1]. This study considers the population of hummingbirds as a feature. The table documenting trips to food sources is configured with the starting values specified in (10).

$$TV_{n,m} = \begin{cases} 0 n \neq m \\ null n = m \end{cases} n = 1, \ldots k; m = 1, \ldots . . k \tag{10}$$

When the $TV_{n,m} = null$, it means that a hummingbird is currently feeding at its assigned food source. For cases where $n \neq m$, $TV_{n,m} = 0$ signifies that the nth hummingbird has just recently visited the mth food source during the current iteration.

ii) Guided foraging

The IAh efficiently integrates and models three types of flight: omnidirectional, diagonal and axial. This is accomplished by incorporating a directional switch vector that controls access to one or several directions in d-dimensional space. The resulting flight behaviors can be extended to describe d-dimensional space, and axial flight is defined in (11).

$$A^n = \begin{cases} 1 if n = ran(1,d) \\ 0 else \end{cases} n = 1, \ldots . d \quad (11)$$

The description of diagonal flight is as in (12).

$$A^n = \begin{cases} 1 if n = s(m), m \in [1,x] s = ranpermutation(h), h \in [2, \lceil r(d-2) \rceil + 1] \\ 0 else \end{cases} n = 1, \ldots . d \quad (12)$$

The description of omnidirectional flight is as in (13).

$$A^n = 1 n = 1, \ldots . d \quad (13)$$

The meaning of $ran(1,d)$ is that it produces a random whole number between 1 and d. Here, $ranpermutation(h)$ generates a random arrangement of integers ranging from 1 to h, and r is a random number that falls between 0 and 1, including 0 and excluding 1. The guided foraging position update is described in (14), while the corresponding stochastic guiding factor is defined in (15).

$$e_n(te+1) = y_{n,aim}(te) + g.A.(y_{n,aim}) \quad (14)$$

$$g \sim ND(0,1) \quad (15)$$

In this context, the equation takes into account $y_n(te)$, which represents the location of the nth food source at time t, $y_{n,aim}(te)$, which signifies the position of the specific food source that the nth hummingbird aims to visit, and a, g guided factor. The value of g is determined by a normal distribution $ND(0,1)$ with a mean of 0 and a standard deviation of 1. The updating of the kth food source's position is described as in (16).

$$y_n(te+1) = \begin{cases} y_n(te) fn(y_n(te)) \leq fn(e_n(te+1)) \\ e_n(te+1) fn(y_n(te)) > fn(e_n(te+1)) \end{cases} \quad (16)$$

Here, $fn(\bullet)$ represents the value of fitness.

iii) Territorial foraging

The mathematical expression describing the local search behavior of hummingbirds in the territorial strategy of food searching on a potential food source is obtained as in (17) and (18).

$$e_n(te+1) = y_{n,aim}(te) + ter.A.(y_{n,aim}) \quad (17)$$

$$ter \sim ND(0,1) \quad (18)$$

Here, ter denotes territorial factor.

iv) Migration foraging

The feeding during migration by a hummingbird that moves from a site of low nectar-refilling rate to a randomly selected new site can be described as in (19).

$$p_{low} = l + r(u-l) \quad (19)$$

Here, P_{low} represents the food source with the least favourable nectar-refilling rate within the population. IAh optimization can be expressed in the following equation.

In (7), r random number replaced by iterative chaotic map. The updated (20) can be expressed in the following manner.

$$A^n = \begin{cases} 1 if n = s(m), m \in [1,x] s = ranpermutation(h), h \in [2, \left\lfloor sin\left(\frac{c\pi}{C_k}\right)(d-2) \right\rfloor + 1] \\ 0 else \end{cases} \quad (20)$$

Here, $c = 0.5$ and Algorithm 1 depict the pseudocode for proposed IAh optimization algorithm. Finally, the proposed model can greatly increase the quality of the deblurring results due to the integration of the IAh optimization algorithm. This way, all important details are retained, and no artifacts are introduced, improving the overall performance of the deblurring model.

Algorithm 1. Pseudocode for IAh optimization algorithm
1: Input: k, l, u, fn, d, max_iter
2: Output: Optimal features are selected
3: **START**
4: **For** n^{th} hummingbird from 1 to k
5: **Do** $P_n = l + r(u - l)$
6: **For** m^{th} food source from 1 to k, **Do**
7: **If** $n \neq m$
8: **Then** $TV_{n,m} = 1$
9: **Else** $TV_{n,m} = null$
10: **End If**
11: **End For**
12: **End For**
13: **While** $te \leq max_iter$**Do**
14: **For** n^{th} hummingbird from 1 to k **Do**
15: **If** $ran \leq 0.5$ **Then**
16: **If** $r < 1/3$**Then** execute (11)
17: **Else If** $r < 2/3$
18: **Then** execute (12)
19: **Else** execute (13)
20: **End If**
21: **End If**
22: Execute equation (14)
23: **If** $fn(e_n(te + 1)) < fn(y_n(te))$
24: **Then** $(y_n(te + 1)) = (e_n(te + 1))$
25: **For**
26: $TV_{n,m} = TV_{n,m} + 1$
27: **End For**
28: $TV_{n,aim} = 0$
29: **For** m^{th} food source from 1 to k
30: **Do**
31: $TV_{m,n} = max\, T\, V_{m,n} + 1$
32: **End For**
33: **Else**
34: **For**m^{th}food source from 1 to $k(m \neq aim, n)$ **Do**
35: $TV_{n,m} = TV_{n,m} + 1$
36: **End For**
37: $TV_{n,aim} = 0$
38: **End**
39: **Else**
40: Execute (17)
41: **If** $fn(e_n(te + 1)) < fn(y_n(te))$
42: **Then** $(y_n(te + 1)) = (e_n(te + 1))$
43: **For**m^{th}food source from 1 to $k(m \neq n)$
44: $TV_{n,m} = TV_{n,m} + 1$
45: **End For**
46: **For** m^{th} food source from 1 to k
47: $TV_{m,n} = max\, T\, V_{m,n} + 1$
48: **End For**
49: **End If**
50: **End If**
51: **End For**
52: **If** $mod(t, 2k) == 0$
53: **Then** execute (19)
54: **For** m^{th}food source from 1 to $k(m \neq low)$ **Do**
55: $TV_{low,m} = TV_{low,m} + 1$
56: **End For**

57: **For** m^{th} food source from 1 to k **Do**
58: $TV_{m,n} = max\, T\, V_{m,n} + 1$
59: **End For**
60: **End If**
61: **End While**
62: **Improve** r random number replaced by iterative chaotic map (20)
63: **STOP**

4. RESULTS AND DISCUSSION

The efficacy of the proposed deblurring method was evaluated by comparison with performance results of existing methods including scale-recurrent network (SRN), deep residual Fourier transformation (DeepRFT) and conventional GANs on blur data obtained from Kaggle. The proposed results were quantified with measures of structural similarity and perceptual quality, including PSNR, SSIM, AMSE, PIQE and spatial and spectral entropy-based quality (SSEQ) measures. These results represent a complete assessment of structural accuracy and perceptual quality for image restoration performance.

Experiments were performed on a machine with Intel(R) Core(TM) i5-3570 CPU @ 3.40 GHz (8 cores) and 8 GB of installed RAM (7.89 GB usable), using a Windows 10 Pro (version 22H2; 64-bit OS). For model training, the hyperparameters were carefully chosen to balance convergence stability and deblurring accuracy. The proposed network used Sigmoid activation, was trained with the adaptive moment estimation (Adam) solver and cross-entropy loss function. The size of kernels was 3 and Adam was used with fixed learning rate = 0.0002. These parameter settings were experimentally confirmed to have robust performance and convergence on different blurred image cases. The proposed IAh-EffGAN showed the best performance among existing GANs models in quantitative and perceptual analysis, by using this experimental configuration and selected hyperparameter.

4.1. Dataset description

The proposed model employs the Blur dataset from Kaggle, available at https://www.kaggle.com/datasets/kwentar/blur-dataset?datasetId=270005 which contains a variety of space-invariant blur types, including defocused blur, sharp blur, and motion blur. The dataset consists of 1,050 images organized into 350 triplets, where each triplet includes three images of the same scene: a sharp reference image, a defocused-blurred image, and a motion-blurred image. Originally curated to validate a blur detection algorithm, this dataset is equally suitable for evaluating image deblurring techniques. The dataset is augmented through horizontal and vertical flipping, rotation (± 15°), and Gaussian noise addition, expanding it to 3,486 training and 523 testing images. This study used Train 3,486 (≈ 87%)/Val 349 (≈ 9.5%) /Test 523 (≈ 13%) with a fixed random seed (42). All models trained on X × Y crops; test metrics were computed on the full-resolution outputs.

The images were collected using 66 different devices, predominantly smartphones but also several digital cameras, thereby ensuring diversity in acquisition quality and conditions. This heterogeneity enhances the dataset's robustness and applicability to real-world scenarios. Figure 5 illustrates representative samples from the Blur dataset.

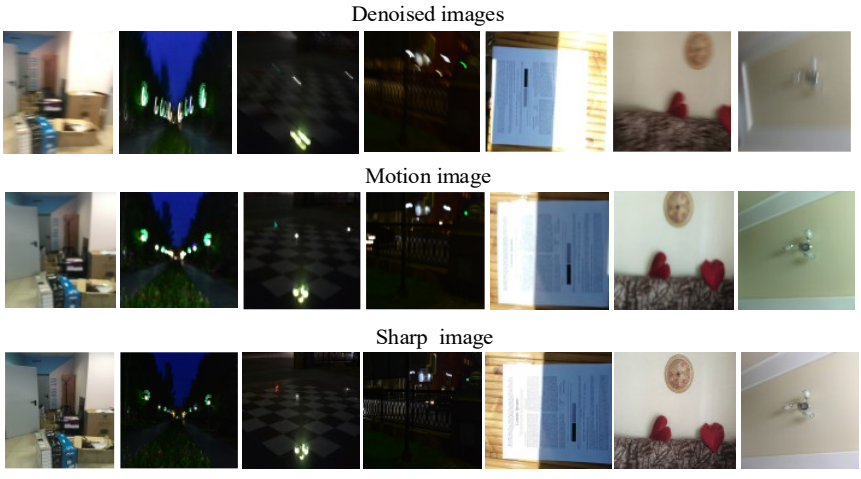

Figure 5. Sample images of "Blur" dataset

4.2. Performance metrics

To assess the effectiveness of the proposed IAh-EffGAN framework, five quantitative evaluation metrics are employed: PSNR, SSIM, AMSE, PIQE, and SSEQ. These metrics provide complementary assessments of reconstruction fidelity, structural preservation, sharpness error, and perceptual image quality. The mathematical formulations and corresponding interpretations of these evaluation metrics are presented in the following subsections.

4.2.1. Peak signal-to-noise ratio

It is the ratio of maximum pixel intensity to the mean square error with respect to the reference image. PSNR is typically measured in decibels (dB), and high PSNR value indicate better image fidelity and lower reconstruction errors. The following is the formulation as in (21).

$$PSNR = 10.log_{10}\left(\frac{MAX^2}{MSE}\right) \tag{21}$$

Here, MAX denotes the maximum possible pixel value for the image, MSE is the mean squared error between the original and reconstructed image, and the PSNR is the ratio of the maximum pixel intensity to the mean squared error.

4.2.2. Structural similarity index measure

This index estimates structural alterations in an image by analyzing luminance, contrast, and the configuration of objects inside it. SSIM scores range from -1 to 1, with 1 signifying perfect similarity. It employs a reference image for structural comparison. The following is the formulation as in (22).

$$SSIM(p,q) = \frac{(2\mu_p\mu_q+G_1)(2\sigma_{p,q}+G_2)}{(\mu_p^2+\mu_q^2+G_1)(\sigma_p^2+\sigma_q^2+G_2)} \tag{22}$$

Here, p and q is denoted as the two input images being compared, μ_p and μ_q is denoted as the mean of p and q, σ_p^2 and σ_q^2 is denoted as the variances of p and q, $\sigma_{p,q}$ is denoted as the covariance of p and q, G_1 and G_2 G_2 is denoted as the small constants added to avoid instability issues with division by 0.

4.2.3. Absolute mean sharpness error

The AMSE measures the average absolute difference in sharpness between corresponding pixels in the reference and test images. A lower AMSE indicates better sharpness similarity between the images. The following is the formulation as in (23).

$$AMSE = \frac{1}{S}\sum_{x=1}^{S}\left|K_{ref}(x) - K_{test}(x)\right| \tag{23}$$

Here, $K_{ref}(x)$ is denoted as the sharpness of the x^{th}pixel in the reference (original) image, $K_{test}(x)$ is denoted as the sharpness of the xth pixel in the test (deblurred) image, and $S$is denoted as the total number of pixels in the image.

4.2.4. Perception-based image quality evaluator

The PIQE metric combines the mean structural similarity index (MSSIM) with a logistic function to evaluate the perceptual quality of the image. It assesses the image quality based on human perception factors and provides a single score that reflects overall image quality. The following is the formulation as in (24).

$$PIQE = \frac{1}{S}\sum_{x=1}^{S}\left(\frac{1}{1+exp(-\beta.(MSSIM(x)-\alpha))}\right) \tag{24}$$

Here, $MSSIM(x)$ is denoted as the MSSIM computed for the xth pixel in the image, α and β is denoted as the scale and sensitivity of the PIQE metric.

4.2.5. Spatial and spectral entropy-based quality

The SSEQ metric computes the combined entropy of spatial and spectral features in the image to assess its quality without relying on reference images. It provides a comprehensive evaluation of image quality based on inherent characteristics such as texture and frequency content. The following is the formulation as in (25).

$$SSEQ = \frac{1}{S}\sum_{x=1}^{S}\left(\frac{T(x)}{T_{max}} + \frac{R(x)}{R_{max}}\right) \quad (25)$$

Here, $T_{(x)}$ and $R_{(x)}$ is denoted as the spatial and spectral entropy of the xth pixel in the image, T_{max} and $R_{max}$is denoted as the maximum spatial and spectral entropy values.

4.3. Performance evaluation of "Blur dataset" analysis

Removing IAh (keeping EfficientNet) reduced PSNR by ≈ 0.7 dB and SSIM by ≈ 0.012; removing EfficientNet (keeping IAh) reduced PSNR by ≈ 0.9 dB and SSIM by ≈ 0.015; removing both decreased PIQE by ≈ 3–4 points. The proposed IAh-EffGAN deblurring model was evaluated against several existing deblurring approaches on the same Blur dataset to demonstrate its performance improvements. For the experiments, a total of 3,486 training images and 523 testing images were utilized to compare the proposed method with both traditional and deep learning–based models. To address computational constraints, the image size was reduced during comparative analysis. This resizing led to minor deviations in results relative to prior studies, which are considered within the acceptable margin of experimental error. On average, the proposed model required 0.32 seconds to process an input image, with 0.23 seconds specifically for deblurring, thereby offering an efficient solution for practical applications.

An essential benefit of IAh-EffGAN is its capacity to proficiently manage both space-variant and space-invariant blur. In contrast to traditional techniques that only tackle invariant blur—characterized by a homogeneous convolution of the blur kernel with the latent image—the proposed framework accommodates more intricate, real-world blur patterns. Figure 6 illustrates a comparative examination of PSNR values, emphasizing the enhanced performance of the proposed model relative to previous methodologies.

Figure 6 shows results of our comparison of PSNR values for our proposed IAh-EffGAN and existing methods of image deblurring are shown. The proposed method produced an average PSNR of 48.344 dB, significantly superior to existing methods that exhibited large errors of reconstruction and reduced performance for both space-invariant and space-variant forms of image blurring. By contrast, IAh-EffGAN restores sharp details more effectively and minimizes artifacts, producing images with greater fidelity and stability across different blur conditions. Although the obtained PSNR values are high, they reflect our patch-based evaluation on aligned triplets with resolution X × Y, artifact suppression via cross-guided bilateral filtering, and reference-aligned crops without compression. The same protocol was used for all models.

Figure 7 presents the analysis of SSIM scores. The proposed model achieves an overall SSIM of 99.05, demonstrating superior preservation of structural details, luminance, and contrast when compared with existing methods. These consistently higher SSIM values confirm the robustness of IAh-EffGAN in maintaining perceptual quality and delivering sharper, more reliable deblurred images. Compared with baseline networks such as SRN and DeepRFT, which generally achieve PSNR in the range of 25–30 dB and SSIM between 0.85–0.92 on similar datasets, the proposed IAh-EffGAN achieves substantially higher reconstruction fidelity and structural consistency.

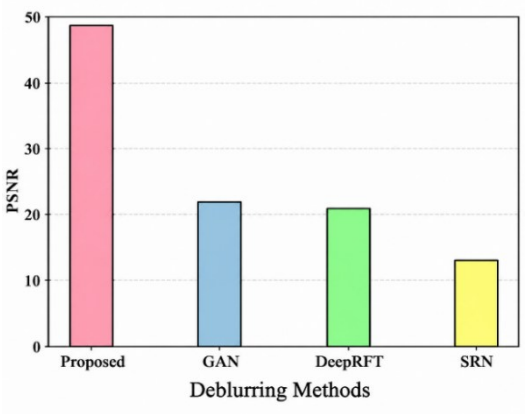

Figure 6. Analysis of PSNR

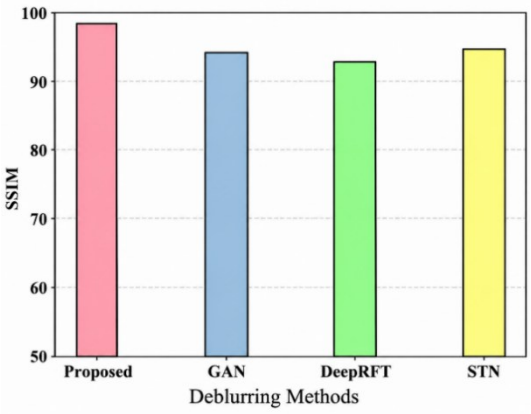

Figure 7. Analysis of SSIM

Figure 8 illustrates the analysis of AMSE for sharp images. The proposed method records an error value of 1.5552, substantially lower than competing models. This reduction highlights its capacity to minimize reconstruction errors and achieve more reliable deblurring outcomes. Figure 9 shows the evaluation

of PIQE performance. The proposed framework attains a score of 98.57, confirming improved sharpness and reduced perceptual distortion compared to existing approaches, which exhibit lower values under both space-variant and space-invariant conditions.

This quantitative improvement is visually evident, as the restored images display enhanced edge continuity and natural texture recovery across motion-blurred and defocused regions. The comparative results for the spectral and spatial entropy-based quality metric SSEQ are shown in Figure 10. The spatial entropy results for the proposed IAh-EffGAN and for existing deblurring methods are presented in Figure 10(a). These results are compared with corresponding spectral entropy results shown in Figure 10(b). The proposed method yielded reduced entropy values, thereby demonstrating improved preservation of image structures and reduced distortion during the deblurring process. The results confirm the ability of the proposed method to maintain both spatial and spectral image quality, and provide additional support for its superiority over conventional methods for all tested quality measures.

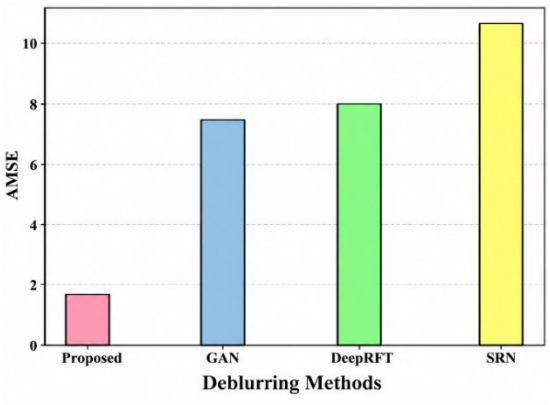

Figure 8. Analysis of AMSE

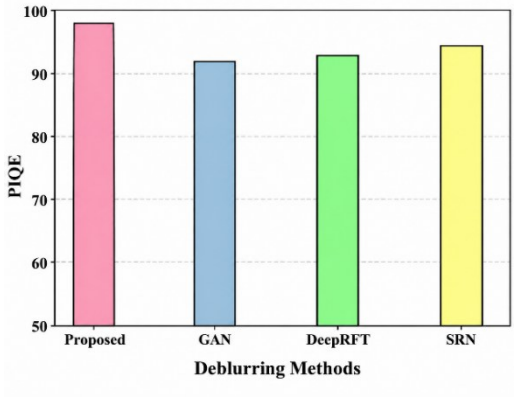

Figure 9. Analysis of PIQE

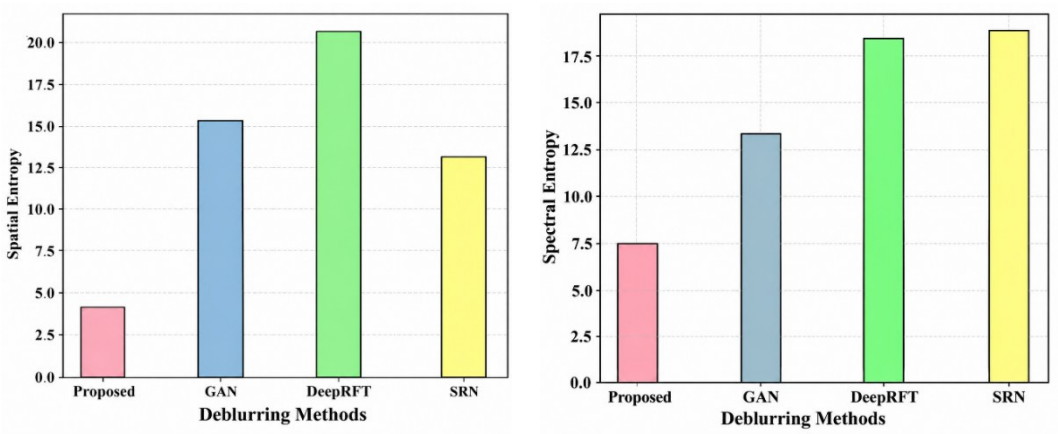

(a) (b)

Figure 10. SSEQ-based comparison of the proposed IAh-EffGAN and existing deblurring models: (a) spatial entropy and (b) spectral entropy

Table 3 presents performance of the proposed and existing models for different classes is compared with respect to PSNR, SSIM, AMSE, and spatial and spectral entropy. The results confirm that the proposed model provides higher performance for all of these measures than the existing model. Table 4 presents results that demonstrate that the limitations of the existing model are effectively overcome with the proposed model and that overall performance for image blur removal is significantly improved. Finally, results for the Blur data set are provided for the filtering and deblurring models.

The suggested model's classification outcome is described in the Table 4. As a result, the different blur and noisy image may be deblurring more precisely and with less time spent. Table 5 depicts deblurring model performance comparison of proposed and existing literature works.

Table 3. Overall deblurring performance in proposed and existing model

Performance	Methods			
	SRN	DeepRFT	GAN	Proposed
PSNR (dB)	13	20.6	21.3	48.344
SSIM (%)	95	93.2	94.4	99.05
AMSE (↓)	11	8	7.5	1.5552
Spatial entropy (↓)	13	20.6	15.3	4.3878
Spectral entropy (↓)	19	18.6	13.3	7.409

Table 4. Blur dataset outcomes of filtering model and deblurring model

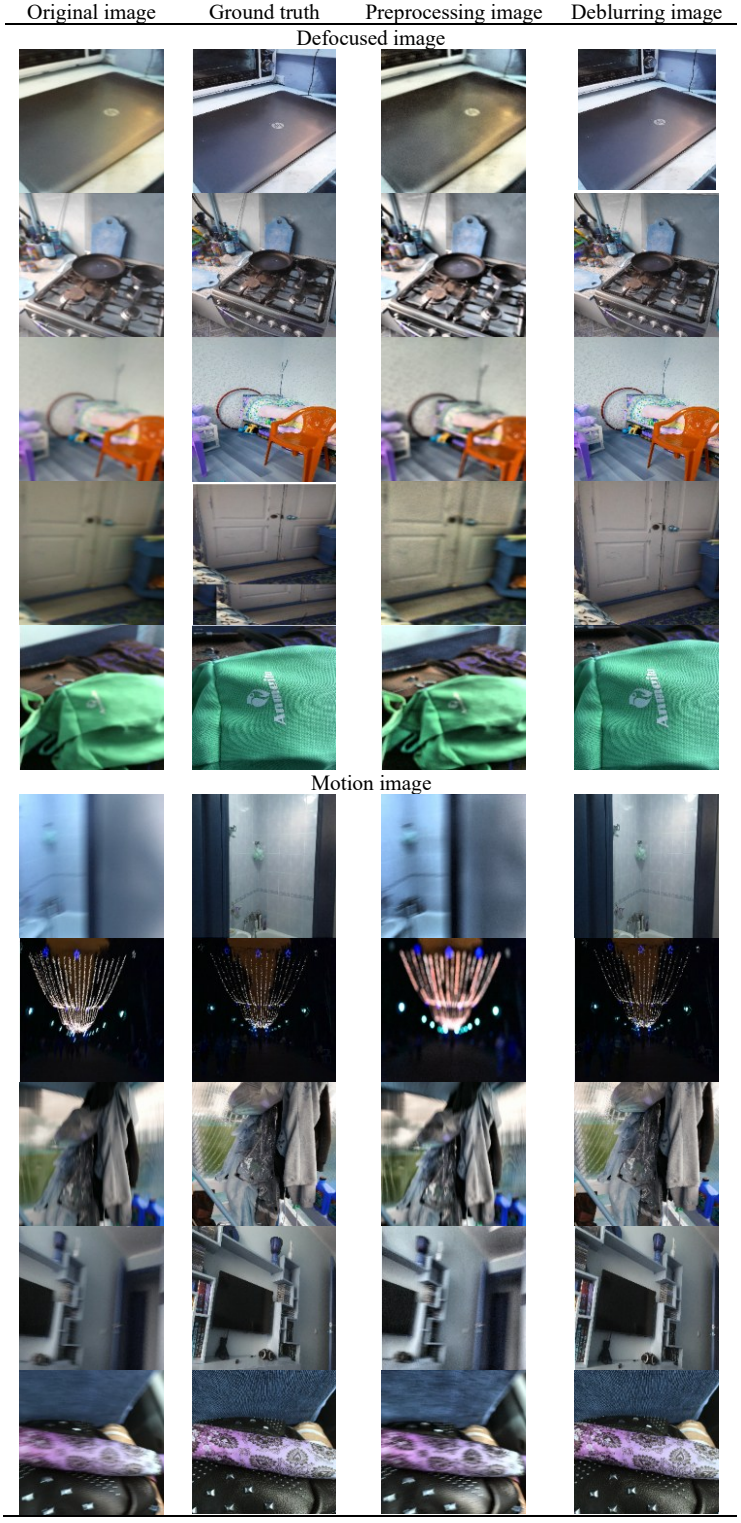

Table 5 cleary shows the evident that the proposed model excels in the task of deblurring. This success can be credited to several factors integrated into the model, such as effective noise and blur reduction, optimized loss functions, superior image quality, and reduced processing time. Together, these results highlight the efficacy of the proposed model in enhancing image deblurring capabilities.

These outcomes affirm the hybrid design's capacity for generalization. By coupling EfficientNet's multi-scale feature encoding with the adaptive exploration of the IAh optimizer, the model maintains convergence stability and high restoration accuracy. The same framework can be extended to related restoration tasks like image super-resolution, inpainting, or denoising under complex real-world conditions.

Table 5. Representative restoration results from related literature

Author and Reference	Method used	Dataset	PSNR (dB)
Guo *et al.* [21]	VDN	GoPro and	31.65
		HIDE	30.09
Zhu *et al.* [22]	AMD-GAN	RealBlur-R	40.58
Souibgui *et al.* [24]	Text-DIAE	IAM,	23.66
		CVL,	23.58
		IIT5K, and	19.95
		IC13	20.0
Kumar and Jain [31]	AI-GAN	Set5	35.58
		Set14	29.92
		B100	28.55
		Urban 100	29.88
		Manga 109	39.99
Jiang and Li [28]	Improved GAN	Set5	30.72
		Set14	28.78
		B100	28.31
		Urban 100	26.51
		Manga 109	28.58
Li and You [32]	SRResNet	Set5	32.11
		Set14	28.52
AlTakrouri *et al.* [33]	image super-resolution generative adversarial network (ISRGAN)-EfficientNet-v2	CIFAR-10	45.56
Wang *et al.* [34]	EGAN	Set5	31.53
		Set14	28.15
		B100	27.41
		Urban 100	25.28
Li *et al.* [35]	Enhanced super-resolution generative adversarial networks (ESRGAN)	BSDS100	25.42
Jiang *et al.* [36]	Depthwise separable convolution super-resolution generative adversarial network (DSCSRGAN)	Set5	30.1438
		Set14	27.11
Gao *et al.* [37]	Conditional generative adversarial network (cGAN)	coco	25.05
Proposed	IAh-EffGAN	Blur dataset	48.34

5. CONCLUSION

This paper introduced an IAh-EffGAN framework for robust deblurring of spatially variant and invariant images. By integrating EfficientNet into a GAN architecture and optimizing its loss using the IAh algorithm, the model demonstrated superior performance on the Blur dataset, achieving a PSNR of 48.344 dB and SSIM of 99.05, clearly outperforming existing methods. The use of a cross-guided bilateral filter further enhanced preprocessing by removing artifacts. Additionally, the cross-guided bilateral filter improved preprocessing by artifact removal. The results of complete evaluations according to PIQE, AMSE, and entropy-based measures verify the model's robustness and generalization capability. Beyond improving image clarity, the approach has potential applications in medical diagnostics, security, and multimedia enhancement. Future work of this study focuses on covering the framework to unsupervised settings, real-time video deblurring, and deployment in edge-AI systems. The IAh-EffGAN framework can be adapted to other restoration tasks such as image super-resolution, inpainting, and real-time deployment in edge-AI systems.

FUNDING INFORMATION

Authors confirmed that there is no funding received for this work.

AUTHOR CONTRIBUTIONS STATEMENT

This journal uses the Contributor Roles Taxonomy (CRediT) to recognize individual author contributions, reduce authorship disputes, and facilitate collaboration.

Name of Author	C	M	So	Va	Fo	I	R	D	O	E	Vi	Su	P	Fu
Rohini Ashok Bhadane	✓	✓	✓	✓	✓	✓		✓	✓	✓			✓	
Amol D. Potgantwar		✓				✓		✓		✓		✓		

C : **C**onceptualization
M : **M**ethodology
So : **So**ftware
Va : **Va**lidation
Fo : **Fo**rmal analysis
I : **I**nvestigation
R : **R**esources
D : **D**ata Curation
O : Writing - **O**riginal Draft
E : Writing - Review & **E**diting
Vi : **Vi**sualization
Su : **Su**pervision
P : **P**roject administration
Fu : **Fu**nding acquisition

CONFLICT OF INTEREST STATEMENT

The authors confirmed that there is no conflict of interest.

DATA AVAILABILITY

The dataset of this study is freely available on the Kaggle website at https://www.kaggle.com/datasets/kwentar/blur-dataset?datasetId=270005.

REFERENCES

[1] B. Maharjan, A. A. Albabawat, R. M. Salah, N. AlSallami, S. Altaf, and O. Al-Jerew, "Augmented reality for cognitive impairment and dementia," in *International Conference on Advances in Computing Research*, 2023, pp. 257–269, doi: 10.1007/978-3-031-33743-7_22.

[2] T. Seizinger, M. V. Conde, M. Kolmet, T. E. Bishop, and R. Timofte, "Efficient multi-lens bokeh effect rendering and transformation," in *2023 IEEE/CVF Conference on Computer Vision and Pattern Recognition Workshops (CVPRW)*, Jun. 2023, pp. 1633–1642, doi: 10.1109/CVPRW59228.2023.00165.

[3] M. V. Conde *et al.*, "Lens-to-lens bokeh effect transformation. NTIRE 2023 challenge report," in *2023 IEEE/CVF Conference on Computer Vision and Pattern Recognition Workshops (CVPRW)*, 2023, pp. 1643–1659, doi: 10.1109/CVPRW59228.2023.00166.

[4] G. F. Torres and J. Kämäräinen, "Depth-aware image compositing model for parallax camera motion blur," in *Image Analysis*. Cham, Switzerland: Springer, 2023, doi: 10.1007/978-3-031-31435-3.

[5] P. Wang *et al.*, "Take a prior from other tasks for severe blur removal," *Computer Vision and Image Understanding*, vol. 245, Aug. 2024, doi: 10.1016/j.cviu.2024.104027.

[6] A. S. Alahmed and S. Ozbay, "Image text deblurring by convolutional neural networks," in *AIP Conference Proceedings*, 2023, doi: 10.1063/5.0103150.

[7] L. G. Varela, L. E. Boucheron, S. Sandoval, D. Voelz, and A. B. Siddik, "Estimation of motion blur kernel parameters usingregression convolutional neural networks," *Journal of Electronic Imaging*, vol. 33, no. 2, pp. 1–16, Apr. 2024, doi: 10.1117/1.JEI.33.2.023062.

[8] G. J. Lakshmi, M. Ghonge, A. J. Obaid, and Muthmainnah, "Generation of masks using nnU-Net framework for brain tumour classification," in *Artificial Intelligence for Smart Healthcare.* Cham, Switzerland: Springer, 2023, pp. 197–209, doi: 10.1007/978-3-031-23602-0_12.

[9] Y. Guo *et al.*, "Blind restoration of a single real turbulence-degraded image based on self-supervised learning," *Remote Sensing*, vol. 15, no. 16, Aug. 2023, doi: 10.3390/rs15164076.

[10] Y. Huihui, L. Daoliang, and C. Yingyi, "A state-of-the-art review of image motion deblurring techniques in precision agriculture," *Heliyon*, vol. 9, no. 6, 2023, doi: 10.1016/j.heliyon.2023.e17332.

[11] Z. Zhang, Y. Cheng, J. Suo, L. Bian, and Q. Dai, "INFWIDE: image and feature space wiener deconvolution network for non-blind image deblurring in low-light conditions," *IEEE Transactions on Image Processing*, vol. 32, pp. 1390–1402, 2023, doi: 10.1109/TIP.2023.3244417.

[12] Z. Fang, F. Wu, W. Dong, X. Li, J. Wu, and G. Shi, "Self-supervised non-uniform kernel estimation with flow-based motion prior for blind image deblurring," in *2023 IEEE/CVF Conference on Computer Vision and Pattern Recognition (CVPR)*, Jun. 2023, pp. 18105–18114, doi: 10.1109/CVPR52729.2023.01736.

[13] S. Cheng, M. Yao, and X. Xiao, "DC-MOT: motion deblurring and compensation for multi-object tracking in UAV videos," in *2023 IEEE International Conference on Robotics and Automation (ICRA)*, May 2023, pp. 789–795, doi: 10.1109/ICRA48891.2023.10160931.

[14] J. Narasimharao, B. Laxmaiah, R. Arumalla, R. Unnisa, T. Fatima, and S. S. Nazare, "Restoration and deblurring the images by using blind convolution method," in *Proceedings of Fourth International Conference on Computer and Communication Technologies: IC3T 2022*, 2023, pp. 337–346, doi: 10.1007/978-981-19-8563-8_32.

[15] A. Upadhyay, J. Li, S. King, and S. Addepalli, "A deep-learning-based approach for aircraft engine defect detection," *Machines*, vol. 11, no. 2, Feb. 2023, doi: 10.3390/machines11020192.

[16] A. Orazaev, P. Lyakhov, V. Baboshina, and D. Kalita, "Neural network system for recognizing images affected by random-valued impulse noise," *Applied Sciences*, vol. 13, no. 3, Jan. 2023, doi: 10.3390/app13031585.

[17] A. A. Al-Dulaimi, M. T. Guneser, A. A. Hameed, F. P. G. Márquez, N. L. Fitriyani, and M. Syafrudin, "Performance analysis of classification and detection for PV panel motion blur images based on deblurring and deep learning techniques," *Sustainability*, vol. 15, no. 2, Jan. 2023, doi: 10.3390/su15021150.

[18] B. N. Chiche, J. N. Girard, J. F.-Pons, A. Woiselle, and J.-L. Starck, "Deep learning-based deconvolution for interferometric radio transient reconstruction," *Astronomy and Astrophysics*, vol. 675, Jul. 2023, doi: 10.1051/0004-6361/202245013.

[19] Y. Zhou, S. Zuo, Z. Yang, J. He, J. Shi, and R. Zhang, "A review of document image enhancement based on document degradation problem," *Applied Sciences*, vol. 13, no. 13, Jul. 2023, doi: 10.3390/app13137855.

[20] B. Ivanov, G. V. Milovanović, and P. S. Stanimirović, "Accelerated Dai-Liao projection method for solving systems of monotone nonlinear equations with application to image deblurring," *Journal of Global Optimization*, vol. 85, no. 2, pp. 377–420, Feb. 2023, doi: 10.1007/s10898-022-01213-4.
[21] C. Guo, Q. Wang, H. Dai, and P. Li, "VDN: variant-depth network for motion deblurring," *Computer Animation and Virtual Worlds*, vol. 33, no. 3–4, Jun. 2022, doi: 10.1002/cav.2066.
[22] B. Zhu, Q. Lv, and Z. Tan, "Adaptive multi-scale fusion blind deblurred generative adversarial network method for sharpening image data," *Drones*, vol. 7, no. 2, Jan. 2023, doi: 10.3390/drones7020096.
[23] S. Karanwal and M. Diwakar, "NABILD: noise and blur invariant local descriptor for face recognition," *Journal of Physics: Conference Series*, vol. 2335, no. 1, Sep. 2022, doi: 10.1088/1742-6596/2335/1/012017.
[24] M. A. Souibgui *et al.*, "Text-DIAE: a self-supervised degradation invariant autoencoder for text recognition and document enhancement," *Proceedings of the AAAI Conference on Artificial Intelligence*, vol. 37, no. 2, pp. 2330–2338, Jun. 2023, doi: 10.1609/aaai.v37i2.25328.
[25] J. Flusser, M. Lébl, F. Šroubek, M. Pedone, and J. Kostková, "Blur invariants for image recognition," *International Journal of Computer Vision*, vol. 131, no. 9, pp. 2298–2315, Sep. 2023, doi: 10.1007/s11263-023-01798-7.
[26] P. Chai, L. Hou, G. Zhang, Q. Tushar, and Y. Zou, "Generative adversarial networks in construction applications," *Automation in Construction*, vol. 159, Mar. 2024, doi: 10.1016/j.autcon.2024.105265.
[27] D. Reyes and J. Sánchez, "Performance of convolutional neural networks for the classification of brain tumors using magnetic resonance imaging," *Heliyon*, vol. 10, no. 3, 2024, doi: 10.1016/j.heliyon.2024.e25468.
[28] Y. Jiang and J. Li, "Generative adversarial network for image super-resolution combining texture loss," *Applied Sciences*, vol. 10, no. 5, Mar. 2020, doi: 10.3390/app10051729.
[29] Y. Zhang *et al.*, "Medical image fusion based on quasi-cross bilateral filtering," *Biomedical Signal Processing and Control*, vol. 80, Feb. 2023, doi: 10.1016/j.bspc.2022.104259.
[30] S. Sarhana, A. Shaheen, R. El-Sehiemy, and M. Gafar, "Optimal multi-dimension operation in power systems by an improved artificial hummingbird optimizer," *Human-centric Computing and Information Sciences*, vol. 13, 2023, doi: 10.22967/HCIS.2023.13.013.
[31] L. Kumar and M. Jain, "A novel image super-resolution reconstruction framework using the AI technique of dual generator generative adversarial network (GAN)," *Journal of Universal Computer Science*, vol. 28, no. 9, pp. 967–983, 2022, doi: 10.3897/jucs.94134.
[32] X. Li and X. You, "End-to-end image super-resolution via generative adversarial network," *IOP Conference Series: Materials Science and Engineering*, vol. 768, no. 7, Mar. 2020, doi: 10.1088/1757-899X/768/7/072063.
[33] S. AlTakrouri, N. M. Noor, N. Ahmad, T. Justinia, and S. Usman, "Image super-resolution using generative adversarial networks with EfficientNetV2," *International Journal of Advanced Computer Science and Applications*, vol. 14, no. 2, 2023, doi: 10.14569/IJACSA.2023.01402100.
[34] Q. Wang, H. Zhou, G. Li, and J. Guo, "Single image super-resolution method based on an improved adversarial generation network," *Applied Sciences*, vol. 12, no. 12, Jun. 2022, doi: 10.3390/app12126067.
[35] C. Li, L. Wang, S. Cheng, and N. Ao, "Generative adversarial network-based super-resolution considering quantitative and perceptual quality," *Symmetry*, vol. 12, no. 3, Mar. 2020, doi: 10.3390/sym12030449.
[36] Z. Jiang, Y. Huang, and L. Hu, "Single image super-resolution: depthwise separable convolution super-resolution generative adversarial network," *Applied Sciences*, vol. 10, no. 1, Jan. 2020, doi: 10.3390/app10010375.
[37] H. Gao, Z. Chen, B. Huang, J. Chen, and Z. Li, "Image super-resolution based on conditional generative adversarial network," *IET Image Processing*, vol. 14, no. 13, pp. 3006–3013, Nov. 2020, doi: 10.1049/iet-ipr.2018.5767.

BIOGRAPHIES OF AUTHORS



Rohini Ashok Bhadane is the research scholar from BKC MET Institute of Engineering, affiliated to Savitribai Phule Pune University, Nashik, Maharashtra, India completed M.E. in Computer Engineering in November, 2015 from K. K. Wagh Institute of Engineering Education and Research, District-Nashik, state-Maharashtra. Since last decade, she working in academics. She can be contacted at email: rohinibhadane102@gmail.com.



Amol D. Potgantwar is the director and professor from the School of Computer Science and Engineering, Sandip University, Nashik, Maharashtra, India. Completed Ph.D. in Computer Science and Engineering, M.Tech. (Computer Science and Engineering), BE (Computer Science and Engineering) and working as a dear IPR and associate professor in the Department of Computer Engineering, Sandip Foundation's, Sandip Institute of Technology and Research Centre, Nashik, Maharashtra, India. He is acting as consultant for many companies nationwide and worldwide and proactive member of Nonprofit Techno Social "Natarajan education society" which emphasizes on mobile applications development for society empowerment and entrepreneurship. He has been a member board of studies in Computer Engineering, at Savitribai Phule Pune University Pune and SGBAU Amravati India. He was convener for 10+ national level STTP like, big data analytics, cloud computing, agile methodology, software testing and IoT. He can be contacted at email: amol.potgantwar@sitrc.org.